Journal of the Technical University of Gabrovo

https://mc04.manuscriptcentral.com/jtug

CONSTRUCTING A ROBOT BASE FRAME CAPABLE OF BALANCING ITS CENTER OF GRAVITY

Dang Anh Viet*

VNU University of Engineering and Technology, Hanoi, Viet Nam

ARTICLE INFO

Article history:
Received 3 March 2026
Revised 25 March 2026
Accepted 30 March 2026

Keywords:
center-of-gravity stabilization, mass redistribution, lead screw mechanism, proportional control, hysteresis logic, robotic platform

ABSTRACT

This study presents the design and experimental validation of a compact robot base frame capable of actively balancing its center of gravity through linear mass redistribution. The system employs a lead-screw-driven sliding counterweight actuated by a NEMA 17 stepper motor and regulated by a real-time proportional controller with hysteresis-based state logic. An analytical moment-balance model establishes the relationship between counterweight mass and maximum compensable load, demonstrating that the balancing capacity is approximately 69% of the counterweight mass under the given geometric constraints. Controller tuning shows that a pure proportional gain $K_p = 40$ achieves a settling time of approximately 16 s with zero overshoot. Experimental multi-load disturbance tests confirm stable bidirectional compensation, accurate load detection within 100 ms, and effective suppression of hunting behavior through a ±100 g deadzone and a 20 g hysteresis band. The results demonstrate that a mechanically simple, single-degree-of-freedom translational mechanism can provide reliable and repeatable mass-based stabilization for compact robotic platforms.

1. INTRODUCTION

Balancing mechanisms play a crucial role in a wide range of engineering systems, including robotic platforms, precision positioning devices, and automated equipment operating under variable load conditions [1-5]. Conventional balance systems often rely on complex multi-axis actuation or sensor-intensive feedback architectures, which increase system cost and implementation complexity [5-10]. In contrast, mass-based stabilization through translational motion offers a mechanically simple and robust alternative for compact systems.

Linear motion mechanisms such as lead-screw-driven actuators are widely adopted in machine design due to their simplicity, load-carrying capability, and positioning accuracy [11-16]. Accordingly, numerous studies have employed computer-aided engineering (CAE) techniques to analyze machine structures with respect to stiffness, strength, vibration, and overall structural integrity. However, these investigations typically treat the mechanical structure as a passive element and focus primarily on structural performance, without considering system-level balancing or active mass redistribution during operation. As a result, the integration of mechanical design with real-time balancing control remains insufficiently explored in existing literature.

To address this gap, this study presents the design, implementation, and experimental validation of a linear-actuated balance system that actively stabilizes the platform by translating a movable mass. The proposed system combines established machine design principles with a real-time control strategy for mass-based stabilization. Unlike simulation-only studies, the system performance is evaluated through experimental tests captured on video, providing direct and intuitive evidence of stability recovery and disturbance rejection.

The main contributions of this work can be summarized as follows. First, a compact balance platform is mechanically designed based on a linear actuator mechanism, in which system stability is achieved through controlled translational motion of a movable mass. Second, a real-time control strategy is implemented to regulate the position of the balancing mass, enabling effective mass-based stabilization under varying conditions. Finally, the balancing performance of the proposed system is experimentally validated using video-based analysis, which provides direct observation of the system's dynamic behavior.

2. MATERIALS AND METHODS

2.1. System overview

Fig. 1 shows the experimental prototype of the proposed linear-actuated balance system, while Fig. 2 presents the corresponding control scheme. The prototype consists of a rigid aluminum frame, a lead-screw-driven sliding counterweight, a linear guide shaft, a NEMA 17 stepper

* Corresponding author. E-mail: vietda@vnu.edu.vn

motor, a TB6600 stepper driver, two load-measurement channels, and a limit-switch-based homing mechanism. The stepper motor drives the lead screw through a flexible coupling, thereby converting rotational motion into translational displacement of the sliding mass platform.

The sensing subsystem is composed of left and right load-measurement channels, each connected to an HX711 signal-conditioning module. The controller acquires the measured loads from both sides of the frame and computes the imbalance signal as the difference between the right and left measured loads. Based on this imbalance, the control algorithm determines both the required direction and speed of counterweight motion. The resulting command is sent to the TB6600 driver, which actuates the NEMA 17 stepper motor. A limit switch is used during startup to establish the home reference and ensure repeatable initial positioning.

This architecture combines a mechanically simple balancing mechanism with a lightweight embedded control implementation. Unlike multi-axis or inertial balancing systems, the proposed prototype relies on a single translational degree of freedom and active mass redistribution, reducing both structural complexity and control cost while retaining effective balancing capability.

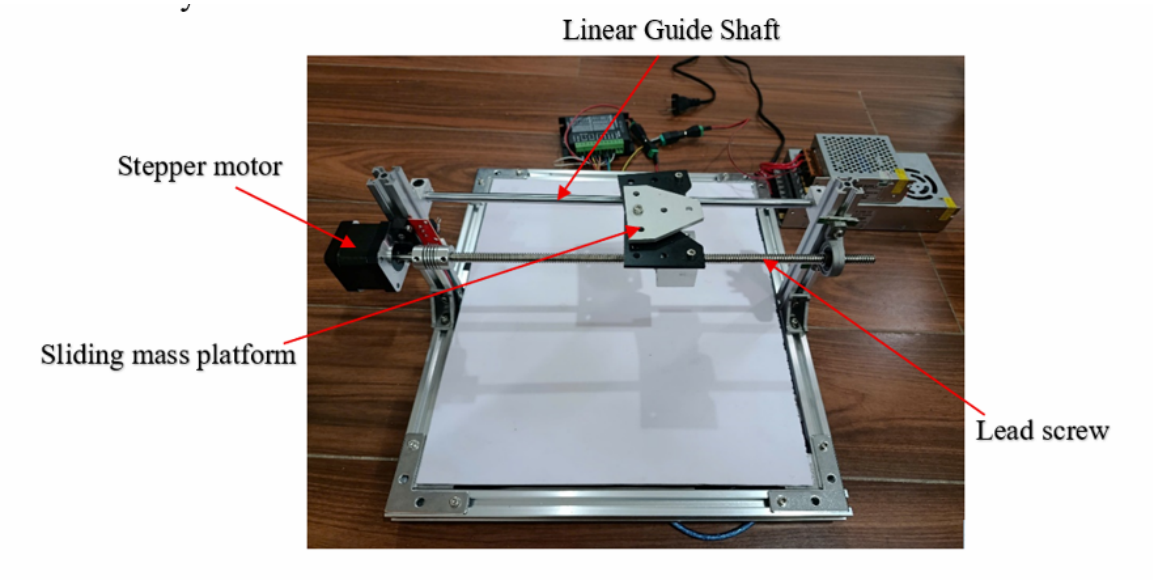

Fig. 1. A prototype of the linear-actuated balance system

2.2. Background and balance principle

The system can be modeled as a rigid frame supported at its center. When an asymmetric load is applied, the resulting moment causes the system to lose equilibrium. Balance is restored by translating a sliding counterweight in the opposite direction to generate a compensating moment.

The static equilibrium condition is expressed as

$$m_{slider} d_{slider} = m_{load} d_{load} \tag{1}$$

where m_{slider} is the mass of the sliding counterweight, d_{slider} is its distance from the frame center, m_{load} is the load imbalance, and d_{load} is the distance from the load application point to the frame center.

Accordingly, the required counterweight position can be written as

$$d_{slider} = \frac{m_{load} d_{load}}{m_{slider}}. \tag{2}$$

For a fixed counterweight mass and limited travel $d_{slider,max}$, the maximum compensable load imbalance is

$$m_{load,max} = \frac{m_{slider} d_{slider,max}}{d_{load}}. \tag{3}$$

In the present prototype, $d_{slider,max} = 120\,mm$ and $d_{load} = 175\,mm$. Therefore,

$$m_{load,max} = \frac{120}{175} m_{slider} \approx 0.69 m_{slider}. \tag{4}$$

Equation (4) provides a direct estimate of the balancing capability for a given counterweight mass.

Table 1 *Balance capability as a function of counterweight mass*

Counterweight mass (g)	***Maximum compensable load imbalance (g)***
200 g	*~ 137 g*
300 g	*~ 206 g*
500 g	*~ 343 g*
1000 g	*~ 686 g*
1500 g	*~ 1029 g*

Table 1 shows that the maximum compensable load imbalance increases linearly with the sliding counterweight mass, in agreement with the analytical moment-balance model given by Eq. (4). Under the present geometric constraints, the maximum compensable imbalance is approximately 69% of the counterweight mass. A 200 g counterweight, used in the experiments, provides sufficient balancing capability for laboratory validation while keeping the actuator demand relatively low. Increasing the counterweight extends the compensation range but also increases actuation torque and power requirements, indicating a trade-off between balancing performance and system complexity.

2.3. Controller tuning procedure

The system was evaluated under controlled laboratory conditions to ensure measurement reliability and repeatability. The ambient temperature was maintained at 25-30°C, the prototype was placed on a flat and rigid ceramic tile surface, and electrical power was supplied from a stable 220 V AC source converted to 12 V DC and 5 V DC for the motor and control circuits, respectively. No significant external vibration was present during testing.

The imbalance was measured using two load-measurement channels corresponding to the left and right sides of the frame. Each channel was connected to an HX711 module for signal conditioning and analog-to-digital conversion. The imbalance signal was computed as

$$\Delta W = W_R - W_L , \quad (5)$$

where W_R and W_L are the right and left measured loads, respectively. In the implemented controller, the measured values were quantized with a 10 g step size to improve robustness against noise and small fluctuations. Calibration was performed using a reference mass before the balancing tests, and no observable cross-talk was found between the left and right channels during the calibration procedure.

The objective of the controller tuning experiment was to identify the best-performing proportional gain within the tested range. Three gain values were evaluated: $K_p = 20$, $K_p = 30$, and $K_p = 40$. In each case, an approximately 200 g load was placed on the left side of the frame, and the balancing process was monitored from activation ([RUN]) to stabilization ([OK]). The motor speed was determined according to the proportional relationship

$$v = K_p |\Delta W| \quad (6)$$

subject to the predefined speed limits of the actuator.

For $K_p = 20$, the system entered the balancing state when the deviation reached -120 g, with a peak deviation of -220 g. The corresponding motor speed ranged between 4000 and 4400 steps/s, and the system returned to the stable region (-80 g) after approximately 25 s. For $K_p = 30$, the peak deviation remained -220 g, the motor speed increased to 6600 steps/s, and the settling time decreased to approximately 21 s. For $K_p = 40$, the theoretical command speed reached 8800 steps/s, but the actual value was limited to 8000 steps/s by the predefined maximum speed. Under this condition, the settling time was reduced to approximately 16 s.

These results show that increasing K_p within the tested range reduces the settling time without introducing overshoot or oscillatory behavior. Therefore, $K_p = 40$ was selected for the subsequent experiments as the best-performing gain among the tested values.

Fig. 2 illustrates the relationship between the proportional gain K_p and the settling time of the balancing system. Increasing K_p from 20 to 40 reduces the settling time from approximately 25 s to 16 s. The improvement is nearly linear within the tested range, indicating that a higher proportional gain strengthens the corrective action and accelerates convergence toward equilibrium. Specifically, increasing K_p from 20 to 30 reduces the settling time by approximately 16%, while increasing it from 20 to 40 achieves a total reduction of approximately 36%. No overshoot or oscillatory behavior was observed for any tested gain value. These results show that $K_p = 40$ provides the best trade-off between response speed and stability within the tested range and was therefore selected for subsequent experiments.

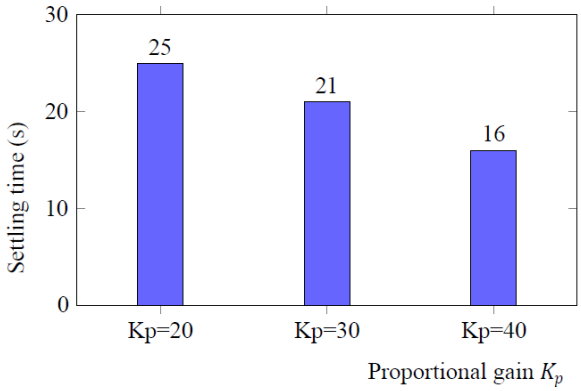

Fig. 2. Settling time as a function of proportional gain K_p

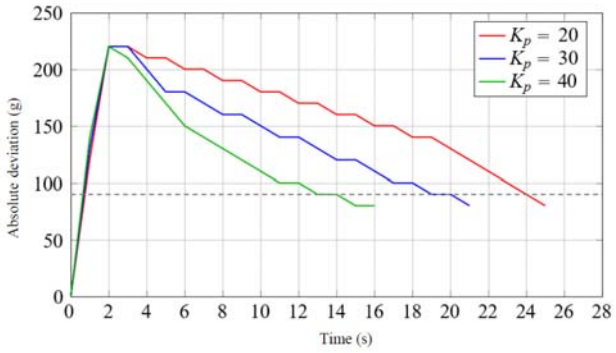

Fig. 3. The time-domain response of the balancing system for three proportional gain values

Fig. 3 presents the time-domain response of the balancing system for three proportional gain values ($K_p = 20$, $K_p = 30$, and $K_p = 40$) under a 200 g load disturbance. In all cases, the deviation initially increased to a peak of approximately 220 g before gradually decreasing toward the equilibrium region. As the proportional gain increased, the rate of deviation reduction became steeper, resulting in shorter settling times. Specifically, $K_p = 40$ achieved the fastest convergence, reaching the deactivation threshold in approximately 16 s, compared with 21 s for $K_p = 30$ and 25 s for $K_p = 20$. No overshoot or oscillatory behavior was observed in any response curve, indicating stable system dynamics under pure proportional control.

3. RESULTS AND DISCUSSION

Table 2 summarizes the system behavior under consecutive and bidirectional load disturbances using the selected proportional gain $K_p = 40$. The experiment began with a centered load after homing, where the deviation remained within the acceptable range ([OK] state). When a 200 g load was added to the left side, a significant negative

deviation (-220 g) was detected, triggering the balancing mode ([RUN]). The system successfully compensated for the imbalance and reduced the deviation to -80 g, returning to the stable state.

Upon removal of the 200 g load, the motor reversed direction automatically, indicating correct detection of deviation sign change and proper bidirectional control capability. Similarly, adding 200 g to the right side produced a large positive deviation that was effectively compensated. The stacked load condition (+200 g on the right combined with +80 g on the left) introduced a more complex imbalance; however, the system maintained stable corrective action without oscillation. Removal of the additional 80 g load resulted in a transient deviation (-110 g), which was again corrected within the acceptable range.

Throughout the entire sequence, the system consistently transitioned between [RUN] and [OK] states according to the hysteresis logic, with no observed instability or overshoot. These results demonstrate the robustness of the proposed balancing mechanism under repeated and varying load conditions.

Table 2 *Experimental timeline under multiple load scenarios*

Time	*Action*	*Deviation (g)*
13:38:46	*Object placed at center after homing*	*L:100, R:110 - +10*
13:39:19	*+200 g added to LEFT side*	*–220 - –80*
13:39:50	*200 g removed from LEFT side*	*Motor reversed direction*
13:40:20	*+200 g added to RIGHT side*	*Large positive deviation*
13:40:50	*+80 g added to LEFT side (stacked load)*	*Slight deviation reduction*
13:41:05	*80 g removed from LEFT side*	*–110 - –80*
13:41:14	*End of experiment*	*L:150, R:70 - –80*

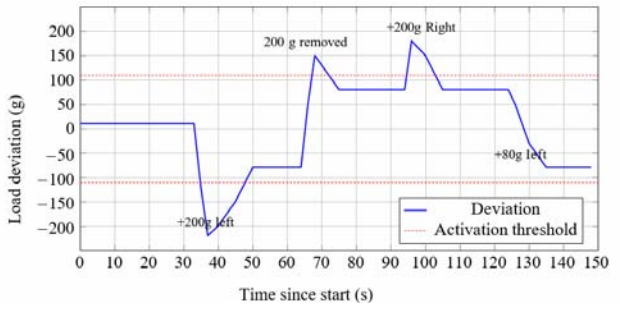

Fig. 4. Deviation response under multi-load disturbances

Fig. 4 shows the time evolution of load deviation during the multi-scenario disturbance test with $K_p = 40$. When a 200 g load was added to the left side, the deviation rapidly reached approximately –220 g, triggering the balancing state. The system progressively reduced the deviation and returned to the acceptable range. Subsequent removal of the load caused a sign reversal, and the controller responded smoothly by reversing motor direction. Similar stable behavior was observed when loads were added to the right side and under stacked loading conditions. In all cases, the deviation was corrected without oscillation or instability, confirming the robustness of the proportional control strategy and the effectiveness of the hysteresis mechanism under repeated bidirectional disturbances.

The experimental results confirm the correct operation of the hysteresis mechanism. The system enters the active balancing state ([RUN]) when the absolute deviation exceeds 110 g and returns to the stable state ([OK]) when the deviation falls below 90 g. This 20 g hysteresis band effectively prevents rapid switching around the threshold. The controller also demonstrates accurate detection of load changes, correct bidirectional compensation, and stable performance under stacked load conditions without noticeable jerk or oscillation.

With the tuned parameters ($K_p = 40$, $K_i = 0$, $K_d = 0$), the controller achieved a settling time of approximately 16 s with zero overshoot and a steady-state deviation within ±90 g. Load changes were detected within 100 ms, and stable operation was maintained without oscillation. The final deviation of -80 g is considered acceptable because it lies within the predefined ±100 g deadzone adopted as the balancing criterion in this study.

4. CONCLUSION

This study presented the design and experimental validation of a compact robot base frame capable of actively balancing its center of gravity through linear mass redistribution. The proposed system combines a lead-screw-driven sliding counterweight, load-cell-based imbalance measurement, and hysteresis-based proportional control in a mechanically simple single-degree-of-freedom configuration.

The analytical model established a linear relationship between counterweight mass and maximum compensable load imbalance, providing a useful basis for system design. Experimental results confirmed that the prototype can maintain stable and repeatable balancing under consecutive, bidirectional, and stacked load disturbances. Among the tested gains, $K_p = 40$ provided the best response within the investigated range.

Overall, the results demonstrate that mass-redistribution-based balancing is a practical solution for compact robotic platforms operating under variable payload conditions. Future work will focus on dynamic disturbances, improved sensing accuracy, and integration into mobile robotic systems.

REFERENCES

[1] Wei B., Zhang D. A Review of Dynamic Balancing for Robotic Mechanisms, Robotica 39(1) (2021) 55-71 http://doi.org/10.1017/S0263574720000168

[2] L. Cui et al., Learning-Based Balance Control of Wheel-Legged Robots, IEEE Robotics and Automation Letters, 6(4) (2021) 7667-7674, Oct. 2021, http://doi.org/10.1109/LRA.2021.3100269

[3] Chen J., He N., Xu Z., Dou M., He L. Design and Implementation of a Novel Two-Wheeled Composite Self-Balancing Robot for Stationary Operations in Unknown Terrain, IEEE Access, 13 (2025) 86032-86045 http://doi.org/10.1109/ACCESS.2025.3569325

[4] Vázquez Muñoz S.D., Ibarra Zannatha J.M., Orozco Soto S.M. Robust Balance of Humanoid Robots Through a LQR with Integral Action, J Control Autom Electr Syst 36 (2025) 34–52 http://doi.org/10.1007/s40313-024-01140-7

[5] Yadav K.P., Narayan J., Kushwaha P. Learning to balance: reinforcement learning control for single-leg balance of an underactuated biped robot, Int. J. Dynam. Controlp 13 (2025) 268 http://doi.org/10.1007/s40435-025-01782-8

[6] Chung Y. -H., Chen Y. -L. Adaptive Vision-Based Method for Rotor Dynamic Balance System, IEEE Access, vol. 9 (2021) 22996-23006, http://doi.org/10.1109/ACCESS.2021.3055257

[7] Vyas Y.J., van der Wijk V., Cocuzza S. A Review of Mechanical Design Approaches for Balanced Robotic Manipulation, Robotics 14 (2025) 151 http://doi.org/10.3390/robotics14110151

[8] Kanellopoulos, D.; Sharma, V.K. Dynamic Load Balancing Techniques in the IoT: A Review. Symmetry 2022, 14, 2554. https://doi.org/10.3390/sym14122554

[9] Harshwerdhan K., Raghuwanshi N. K., Singh A. K. Optimal dynamic balancing of rotating mechanical system using equimomental mass redistribution, Mechanics Based Design of Structures and Machines, 54(1) (2026) http://doi.org/10.1080/15397734.2026.2627625

[10] Raza F., Zhu W., Hayashibe M. Balance Stability Augmentation for Wheel-Legged Biped Robot Through Arm Acceleration Control, IEEE Access, 9 (2021) 54022-54031 http://doi.org/10.1109/ACCESS.2021.3071055

[11] Tung T.T., Anh N.T., Minh T.V. Design and development of a prototype 3-axis CNC wood carving machine. International Journal of Advanced Technology and Engineering Exploration 12(125) (2025) 528-541 http://doi.org/10.19101/IJATEE.2024.111101739

[12] Tung Tran Thanh, Vu Minh Tran. Development of a prototype pineapple peeling machine, International Journal of Advanced Technology and Engineering Exploration 11(114) (2024) 795 http://doi.org/10.19101/IJATEE.2023.10102547

[13] Kumar J. et al. Design and fabrication of 3-axis CNC milling machine using additive manufacturing, Materials Today: Proceedings 68 (2022) 2443-2451 http://doi.org/10.1016/j.matpr.2022.09.145

[14] Das Utpal Chandra et al. Development of automatic CNC machine with versatile applications in art, design, and engineering., Array 24 (2024)100369 http://doi.org/10.1016/j.array.2024.100369

[15] Tung T.T., Anh N.T., Quynh N.X., Minh T.V. Simulation and Experimental Study of a Lightweight Pick-and-Place Robotic Arm Prototype, Journal of Integrated Science and Technology, 14(1) (2026) 1511 http://doi.org/10.62110/sciencein.jist.2026.v14.1511

[16] Zaier R., AlYahmedi A.S. Adaptive Screw-Drive In-Pipe Robot with Hall-Effect Force Sensing and Active Gripping Control, Electronics 15 (2026) 960 http://doi.org/10.3390/electronics15050960

[17] Nguyen Thi Anh, Tran Thanh Tung. Development of Flexible Clamping Devices for Precision Workholding of Irregular and Thin-Walled Workpieces, International Journal of Mechanical Engineering and Robotics Research, 14(6) (2025) 676-684 http://doi.org/10.18178/ijmerr.14.6.676-684

[18] Kondo A., Hayashi H., Toyoshi T. Project-Based Learning of Mechanical Design Utilizing CAE Structural Analyses, Educ. Sci. 13 (2023) 687 http://doi.org/10.3390/educsci13070687

[19] Guzmán-Siles A., Tovar-Martínez E., Navarro-Rojero M.G., Mercado-Lemus V.H., Betancourt-Cantera J.A., Pereyra I., González-López M.Á., Mayén-Chaires J., Garduño I.E., del Ángel-Monroy M. Optimization of Metallic Support Geometry for Automotive Doors Using CAD, CAE, and Taguchi Method to Improve Structural Rigidity, Eng 6 (2025) 361 http://doi.org/10.3390/eng6120361

[20] Yoo S., Lee S., Kim S. et al. Integrating deep learning into CAD/CAE system: generative design and evaluation of 3D conceptual wheel, Struct Multidisc Optim 64 (2021) 2725–2747 http://doi.org/10.1007/s00158-021-02953-9

[21] Huang C.M., Kucinic A., Johnson J.A. et al. Integrated computer-aided engineering and design for DNA assemblies. Nat. Mater. 20 (2021) 1264–1271 http://doi.org/10.1038/s41563-021-00978-5

[22] Anh Nguyen Thi, Tran Thanh Tung. Design and Manufacture of a Cutting Force Measuring Device for a 3 Axis CNC Milling Machine, Next Research (2026) 101549 http://doi.org/10.1016/j.nexres.2026.101549

[23] Chan TC., Ullah A., Roy B. et al. Finite element analysis and structure optimization of a gantry-type high-precision machine tool. Sci Rep 13 (2023) 13006 http://doi.org/10.1038/s41598-023-40214-5

[24] Kouritem Sallam A. et al. A multi-objective optimization design of industrial robot arms, Alexandria Engineering Journal 61(12) (2022) 12847-12867 http://doi.org/10.1016/j.aej.2022.06.052